Nanoscale Advances

PAPER

View Article Online
View Journal | View Issue

Cite this: *Nanoscale Adv.*, 2022, **4**, 5132

Surface-passivated Cu conductors for high-temperature sulfurous environments†

Zheng Li,[a] Jian Yu,[b] Saurabh Khuje,[a] Aaron Sheng,[a] Marieross Navarro,[a] Cheng-Gang Zhuang[c] and Shenqiang Ren *[ade]

Received 13th July 2022
Accepted 22nd October 2022

DOI: 10.1039/d2na00452f

rsc.li/nanoscale-advances

Advanced materials capable of withstanding extreme environments garner extensive interest in the development of next-generation advanced anti-corrosion electronics. Herein, we report that the surface passivation of printed copper conductors imparts corrosion resistance in high-temperature sulfurous environments while maintaining a high electrical conductivity of 4.42 MS m^{-1} when subjected to a sulfur-containing environment at 350 °C for 12 h. This study provides potential for the development of surface-passivated copper conductors that are resistant to the sulfidizing environments found in several applications of modern technology.

Introduction

The corrosion of metallic materials is more acute when they are continuously exposed to atmospheres containing sulfur at elevated temperatures than in oxidizing environments.[1] If the partial pressure of sulfur is low in atmospheres with a high amount of combustion gases, such as those found in energy-conversion processes, sulfur is unlikely to corrode oxidation-resistant metals/alloys. However, these oxidation-resistant metals/alloys undergo rapid deterioration in high-sulfide environments, particularly under high temperature, where even a trace of sulfur can cause catastrophic deterioration.[2] Consequently, several strategies have been employed to improve the corrosion resistance of metals against sulfide corrosion in high-temperature applications. One strategy is to pre-oxidize the metal, which favors the formation and adhesion of a dense chromia or alumina coating with no physical defects on the core material.[3] However, if the structural integrity is compromised in harsh environments, such as those found on Venus with its reactive sulfuric environment and high average surface temperature, corrosion could occur at high rates, destabilizing the structure and electrical conductivity of the metal components in electronic devices.[4–7] Another strategy is to utilize high-temperature metallic materials for corrosion-resistant electronics,[8] including noble metals, such as gold,[9] silver,[10] and palladium,[11] and passive metals, such as nickel.[12] Such high-temperature conductors offer high melting points, good electrical performance, and low heat expansion coefficients. However, prolonged exposure to a sulfur atmosphere could cause a 16% mean increase in resistance, with up to 30% at 150 °C. Therefore, it is necessary to seek alternative materials.[13–15]

Metallic copper (Cu) provides high electrical and thermal conductivity;[16,17] however, oxidation and corrosion resistance treatments involving alloying often compromise its electronic and thermal conductivity.[18–20] To address these issues, enormous efforts have been devoted to using a robust and dense passivating layer to shield the conductor, enabling it to withstand extreme environments.[21,22] Generally speaking, resistance to sulfur corrosion is achieved by applying a polymer coating on the Cu surface,[23] such as resins, epoxy, and polyamides. However, these polymers are vulnerable to hydrolysis and degradation, and are not able to survive under high temperatures. Chitosan-based coatings[24] and (2*E*,5*E*)-bis[(4-dimethylamino)benzylidene]cyclopentanone[25] have also been investigated as corrosion inhibitors for Cu substrates under aqueous sulfuric acid. Chilkoor *et al.* coated Cu with hexagonal boron nitride (hBN) to prevent corrosion from sulfur compounds, and Cu–hBN showed seven times lower corrosion than bare Cu at room temperature.[26] Here, we report the effective surface passivation of printed Cu conductors on Corning flexible Alumina Ribbon Ceramic to endow it with stability under high-temperature sulfur-containing environments. As shown in Fig. 1, the printed conductors examined in this study include a Cu/graphene physical mixture (Cu/G),[27,28] hybridized Cu–graphene (Cu–G) from the *in situ* conversion of copper–dopamine complexes, and Cu featuring a conformal Al_2O_3

[a]*Department of Mechanical and Aerospace Engineering, University at Buffalo, The State University of New York, Buffalo, New York, 14260, USA. E-mail: shenren@buffalo.edu*

[b]*DEVCOM Army Research Laboratory, Aberdeen Proving Ground, MD, 21005, USA*

[c]*Corning Research and Development Corporation, New York, 14830, USA*

[d]*Department of Chemistry, University at Buffalo, The State University of New York, Buffalo, New York, 14260, USA*

[e]*Research and Education in Energy Environment & Water Institute, University at Buffalo, The State University of New York, Buffalo, New York, 14260, USA*

† Electronic supplementary information (ESI) available. See DOI: https://doi.org/10.1039/d2na00452f

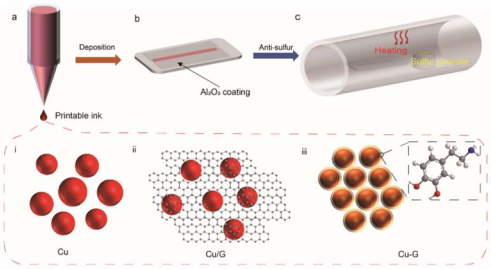

Fig. 1 Schematic of the Cu-based conductor for sulfur corrosion resistance. (a) Printing of the Cu-based conductors: Cu NPs (i), Cu/G (ii), and Cu–G (iii). (b) Cu-based conductor with a thin Al_2O_3 layer coating. (c) Schematic of *in situ* measurement under a sulfurous atmosphere at different temperatures.

coating (Cu–Al_2O_3). We selected polydopamine, which can be carbonized at elevated temperatures in an inert atmosphere, to serve as a potent source of graphene in the printed Cu–G conductor, as it can form an adherent coating on the copper surface owing to its amine (–NH_2) and hydroxyl (–OH) functional groups.[27] Moreover, polymerization being an oxidative process helps in reducing surface oxides on the printed copper surface during the annealing step. In addition, we deposited an Al_2O_3 passive coating on printed copper, which serves as a defensive shield between copper and the corrosive environment. The as-fabricated graphene passivation layer and conformal Al_2O_3 coating provide oxidation and corrosion resistance to the printed Cu conductors under a high-temperature sulfurous atmosphere, while maintaining its high electrical conductivity of 4.42 MS m^{-1}.

Experimental section

Synthesis of Cu NPs

First, the capping polymer polyvinylpyrrolidone (PVP) and reducing agent sodium phosphinate monohydrate ($NaH_2PO_2 \cdot H_2O$) were dissolved in diethylene glycol (DEG) *via* heating and stirring. When the solution temperature reached 140 °C, aqueous copper sulfate was injected uniformly into the hot DEG solution *via* a syringe pump for the reaction. Then, the solution was naturally cooled to room temperature and copper nanoparticles (Cu NPs) were obtained by centrifugation. Finally, the Cu NPs were cleaned with methanol four times to remove any impurities. During the synthesis of Cu NPs, the PVP content and reaction time were varied to investigate their effects on the NP size.

Printing Cu-based conductors

Hydroxypropyl methylcellulose (HPMC) solution (2 wt% in deionized water) and copper ink feedstock collected through centrifugation were mixed using an ARE-310 Thinky Mixer to prepare the conductive ink. Cu/G or Cu–G inks were prepared *via* the addition of graphene (5 wt% of the ink) or dopamine (5 wt% of the ink), respectively, and mixed to obtain a uniform ink. The printing of conductive ink was performed on a direct writing or ink-jet printer. Subsequently, the printed conductors coated onto Corning flexible Alumina Ribbon Ceramic were sintered under 95% nitrogen and 5% hydrogen at different temperatures to facilitate the removal of residual organics. Furthermore, polydopamine was converted to graphene *in situ* under high-temperature and forming gas conditions.

Atomic layer deposition

A Savannah S100 atomic layer deposition (ALD) setup was used to deposit ultrathin Al_2O_3 films. The trimethylaluminum (TMA) precursor and H_2O were sequentially exposed for 0.015 s with 8 s waiting time between the respective cycles and nitrogen purging at a rate of 20 sccm. The number of cycles was based on the desired thickness, and a thickness of 100 nm was deposited onto the printed feature on the flexible substrate. The deposition temperature was 200 °C.

Morphological and structural characterization

Transmission electron microscopy (TEM) images were acquired on a JEOL JEM 2010 high-resolution TEM instrument. Scanning electron microscopy (SEM) and energy-dispersive X-ray spectroscopy (EDS) mapping images were captured on a ZEISS crossbeam FIB-SEM and Oxford EDS system, respectively. An SDT Q600 thermogravimetric analyzer was used to generate TGA curves. X-ray diffraction (XRD) patterns were recorded on a Rigaku Ultima IV instrument at a step of 5° min^{-1}. The electrical characteristics were recorded on a Keithley 2450 source meter.

Results and discussion

The printability and sintering profiles of Cu NPs depend on their synthesis-controlled dimensions obtained through the polyol process,[29,30] involving diethylene glycol (DEG) as the solvent, polyvinylpyrrolidone (PVP) as the capping molecule, and sodium phosphinate monohydrate ($NaH_2PO_2 \cdot H_2O$) as the reducing agent (Fig. 2a). As shown in Fig. 2b and c, the average size of the Cu NPs was 100 nm, and could be tuned by varying the amount of the encapsulating ligand PVP and reaction time

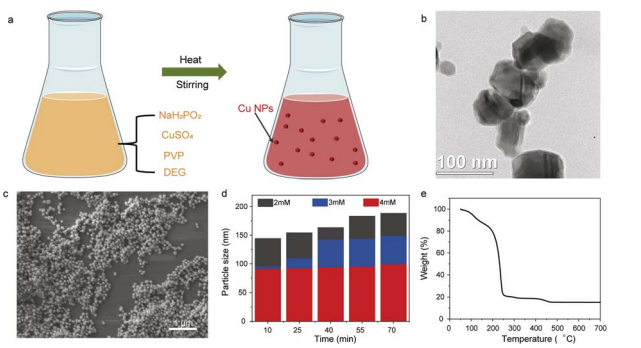

Fig. 2 Structure and morphology of the Cu NPs. (a) Synthetic route of the Cu NPs. (b) TEM image of the Cu NPs. (c) SEM image of the Cu NPs. (d) Cu NP size distribution derived from image analysis. Reaction time and PVP concentration dependence of the particle size of the Cu NPs. (e) TGA curve of the printable Cu ink.

(Fig. S1†). When the concentration of PVP was 2 mM, the average size of the Cu NPs ranged from 140 nm to 170 nm with the reaction time increasing from 10 min to 70 min (Fig. 2d). On increasing the PVP content to 3 mM, the average size of the Cu NPs increased from 95 nm to 145 nm under the reaction times of 10 min to 70 min. This suggests that the PVP ligand suppresses the growth and agglomeration of Cu NPs, while the size of the Cu NPs is controlled by the reaction time. Thermogravimetric analysis (TGA, Fig. 2e) of the printable Cu nanoparticle ink materials confirmed that the Cu solid content was about 20 wt%, with the decomposition of the organic ligand at 250 °C.

The Cu NP inks were printed *via* both direct writing and ink-jetting onto different flexible substrates (paper, Kapton®, and Corning flexible Alumina Ribbon Ceramic; Fig. 3a and b). As shown in Fig. 3c, the electrical conductivity of the printed Cu features increased from 0.5 MS m^{-1} to 4.6 MS m^{-1} on increasing the sintering temperature from 250 °C to 850 °C, where the Cu NPs exhibited both sintering necks and long-range connections. Similar behavior was observed for the printed Cu/G and Cu–G conductors, whose electrical conductivities were 3.5 MS m^{-1} and 3.3 MS m^{-1} after heat treatment at 850 °C, respectively. It is worth noting that the sintering time is another key factor influencing electrical conductivity. Increasing the sintering time from 5 to 20 min at 250 °C increased the conductivity of the printed Cu features from 0.15 MS m^{-1} to 0.5 MS m^{-1}, and then to 0.52 MS m^{-1} with a sintering time of 30 min (Fig. 3d). It was also observed that as the annealing temperature increased to 550 °C and 850 °C, the conductivity of the Cu conductor showed a subtle increase with increase in annealing time.

The sulfur-corrosion resistance of the Cu-based conductors was examined by evaluating the reliability of electric conductivity under a sulfurous atmosphere at various temperatures.[31] Fig. S2† and 4a present the time-dependent conductivity of the printed Cu-based conductors (Cu, Cu/G, Cu–G, and Cu–Al_2O_3) at 35 and 150 °C, respectively. The conductivity of Cu decreased to 20% of its initial value after exposure to sulfur atmosphere at 35 °C for 10 min, and then broke after 60 min due to reaction with sulfur to form copper sulfide. Furthermore, the printed Cu conductors subjected to 10 min exposure to the sulfur atmosphere at 150 °C were quickly corroded by sulfur and became non-conductive. This was further confirmed by SEM and EDS elemental mapping images before (Fig. 4b) and after (Fig. 4c) sulfur corrosion. EDS indicated that these needle-like crystals were mainly composed of copper sulfide. Similarly, XRD analysis of the printed copper conductors before and after sulfur corrosion also confirmed the formation of copper sulfide (Fig. S3†). Graphene incorporation into the Cu conductors (both Cu/G and Cu–G) exhibited sulfur-corrosion resistance below 60 min. After exposure to a sulfurous atmosphere for 10 min at 150 °C, the conductivity of the Cu/G conductor decreased to 78% of its initial value, while the conductivity of the Cu–G conductor decreased by only 11%, indicating that the *in situ*-formed graphene passivation provided enhanced protection from sulfur corrosion. Fig. S4† shows the SEM and EDS images of the Cu/G conductor before and after sulfur corrosion. It is worth noting that the copper with a conformal Al_2O_3 coating layer with a thickness of 100 nm (Fig. 4d and S5†) showed no change in morphology before and after exposure to the

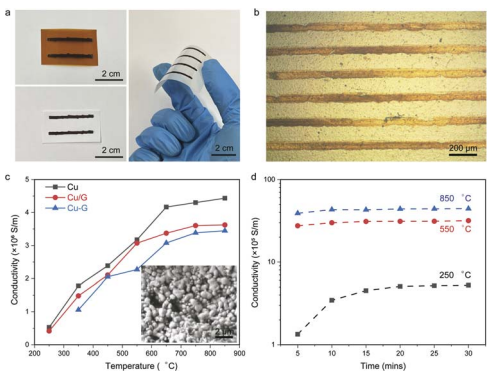

Fig. 3 Conductivity of the printed Cu-based conductor. (a) Picture of the printed Cu conductor on flexible Kapton®, paper and ceramic substrate *via* direct writing. (b) Ink-jet printing of the Cu conductor on the Kapton® substrate. (c) Electrical conductivity as a function of sintering temperature. Inset is an SEM image of the Cu NPs after sintering at 850 °C. (d) The plot of Cu NP conductivity *versus* sintering time at 250 °C, 550 °C and 850 °C.

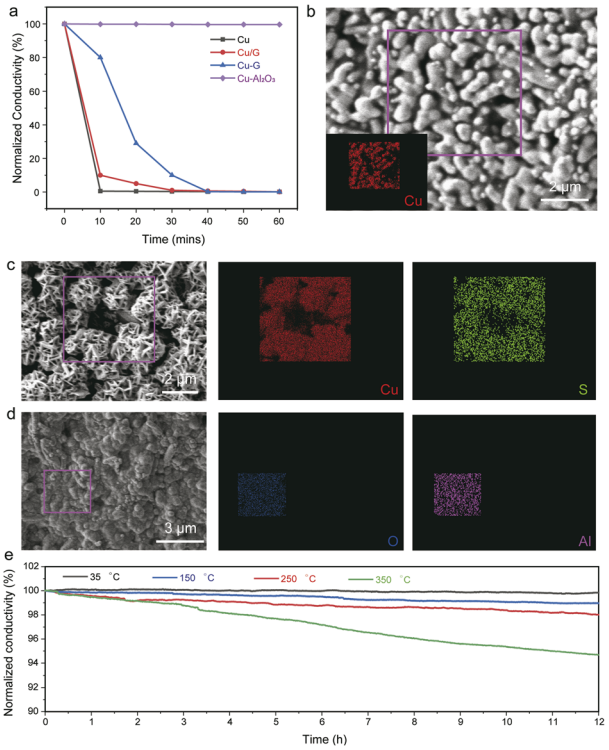

Fig. 4 Cu-based conductor performances under sulfurous atmosphere. (a) Conductivity changes of the Cu-based conductors (Cu, Cu/G, Cu–G and Cu–Al_2O_3) at 150 °C under sulfurous atmosphere. (b) SEM image of Cu before the test. Inset is the EDS mapping. (c) SEM and EDS images of Cu after the test. (d) SEM and EDS images of Cu–Al_2O_3 after the test. (e) Conductivity changes of Cu–Al_2O_3 at different temperatures for 12 h.

sulfurous atmosphere, indicating that the Al_2O_3 coating protected the printed copper. Printed copper with Al_2O_3 coating showed robust sulfur resistance at 35 °C for more than 12 h, with a slight conductivity change of only 1% (Fig. 4e). When the temperature was increased to 150, 250 and 350 °C, the Cu–Al_2O_3 conductor maintained its reliability over 12 h, with the conductivity retention exceeding 95%, suggesting that this is a promising strategy to passivate Cu conductors to survive high-temperature sulfur environments.

Conclusion

In summary, the surface passivation of printed Cu-based conductors with graphene (physical mixing and *in situ* conversion) or an Al_2O_3 passivating layer afforded corrosion resistance under a high-temperature sulfurous atmosphere. The synthesized nanoparticles that formed the basis of this study could be printed using direct writing or ink-jetting onto different substrates, and the conductivity of the Cu NP conductor showed an increasing trend with increasing sintering temperature. When the printed conductor with a conformal 100 nm Al_2O_3 coating was exposed to a sulfur-containing environment at 350 °C for 12 h, the change in electric conductivity of the printed Cu conductor was less than 5%, maintaining a value of about 4.42 MS m^{-1}. The proposed strategy provides the potential to extend the stability of copper conductors under extreme environments.

Conflicts of interest

There are no conflicts to declare.

Acknowledgements

Financial support was provided by the DEVCOM Army Research Laboratory, which supports S. R. under Award W911NF-20-2-0016 (conductive ink materials). High-temperature printable hybrid electronics is based on research sponsored by NextFlex through the Air Force Research Laboratory under Agreement Number FA8650-20-2-5506. The U.S. Government is authorized to reproduce and distribute reprints for governmental purposes notwithstanding any copyright notation thereon. The views and conclusions contained herein are those of the authors and should not be interpreted as necessarily representing the official policies or endorsements, either expressed or implied, of the Air Force Research Laboratory or the U.S. Government.

References

1 D. Meadowcroft and M. Manning, *Corrosion Resistant Materials for Coal Gasification Systems*, Applied Science, London, 1982.
2 S. Mrowec, *Oxid. Met.*, 1995, **44**, 177–209.
3 N. R. C. o. Canada, *Compte rendu*, National Research Council of Canada, 1984.
4 C. A. Sequeira, *High Temperature Corrosion: Fundamentals and Engineering*, John Wiley & Sons, 2019.
5 D. Lukco, D. J. Spry, P. G. Neudeck, L. M. Nakley, K. G. Phillips, R. S. Okojie and G. W. Hunter, *J. Spacecr. Rockets*, 2020, **57**, 1118–1128.
6 P. G. Neudeck, L. Chen, R. D. Meredith, D. Lukco, D. J. Spry, L. M. Nakley and G. W. Hunter, *IEEE J. Electron Devices Soc.*, 2019, **7**, 100–110.
7 M. J. Schuster, S. G. Brunner, K. Bussmann, S. Buttner, A. Domel, M. Hellerer, H. Lehner, P. Lehner, O. Porges, J. Reill, S. Riedel, M. Vayugundla, B. Vodermayer, T. Bodenmuller, C. Brand, W. Friedl, I. Grixa, H. Hirschmuller, M. Kassecker, Z. C. Marton, C. Nissler, F. Ruess, M. Suppa and A. Wedler, *J. Intell. Rob. Syst.*, 2019, **93**, 461–494.
8 A. Sheng, S. Khuje, J. Yu, D. Petit, T. Parker, C. G. Zhuang, L. Kester and S. Ren, *Nano Lett.*, 2021, **21**, 9279–9284.
9 C. W. Corti and R. J. Holliday, *Gold Bull.*, 2004, **37**, 20–26.
10 T. Duy and H. Seo, *Appl. Surf. Sci.*, 2020, **521**, 146467.
11 J. L. Tang, Z. H. Zhang, Y. Y. Wang, P. F. Ju, Y. M. Tang and Y. Zuo, *Corros. Sci.*, 2018, **135**, 222–232.
12 Y. K. Wei, Y. J. Li, Y. Zhang, X. T. Luo and C. J. Li, *Corros. Sci.*, 2018, **138**, 105–115.
13 R. He, Y. C. Wang, X. Wang, Z. Wang, G. Liu, W. Zhou, L. Wen, Q. Li, X. Wang, X. Chen, J. Zeng and J. G. Hou, *Nat. Commun.*, 2014, **5**, 4327.
14 M. Grouchko, A. Kamyshny and S. Magdassi, *J. Mater. Chem.*, 2009, **19**, 3057–3062.
15 J. Peng, B. Chen, Z. Wang, J. Guo, B. Wu, S. Hao, Q. Zhang, L. Gu, Q. Zhou, Z. Liu, S. Hong, S. You, A. Fu, Z. Shi, H. Xie, D. Cao, C. J. Lin, G. Fu, L. S. Zheng, Y. Jiang and N. Zheng, *Nature*, 2020, **586**, 390–394.
16 A. R. Rathmell, M. Nguyen, M. Chi and B. J. Wiley, *Nano Lett.*, 2012, **12**, 3193–3199.
17 Z. Chen, S. Ye, I. E. Stewart and B. J. Wiley, *ACS Nano*, 2014, **8**, 9673–9679.
18 W. Shinato, A. A. Zewde and Y. Jin, *Corros. Rev.*, 2020, **38**, 101–109.
19 T. G. Kim, H. J. Park, K. Woo, S. Jeong, Y. Choi and S. Y. Lee, *ACS Appl. Mater. Interfaces*, 2018, **10**, 1059–1066.
20 S. J. Eder, P. G. Grutzmacher, M. Rodriguez Ripoll, D. Dini and C. Gachot, *Materials*, 2020, **14**, 60.
21 G. Dingemans and E. Kessels, *J. Vac. Sci. Technol., A*, 2012, **30**, 040802.
22 L. Kovarik, M. Bowden, A. Andersen, N. R. Jaegers, N. Washton and J. Szanyi, *Angew. Chem., Int. Ed. Engl.*, 2020, **59**, 21719–21727.
23 Z. P. Kopteva, V. V. Zanina and I. A. Kozlova, *Surf. Eng.*, 2004, **20**, 275–280.
24 C. Giuliani, M. Pascucci, C. Riccucci, E. Messina, M. S. de Luna, M. Lavorgna, G. M. Ingo and G. Di Carlo, *Prog. Org. Coat.*, 2018, **122**, 138–146.
25 V. Thaçi, R. Hoti, A. Berisha and J. Bogdanov, *Open Chem. J.*, 2020, **18**, 1412–1420.
26 G. Chilkoor, K. Jawaharraj, B. Vemuri, A. Kutana, M. Tripathi, D. Kota, T. Arif, T. Filleter, A. B. Dalton, B. I. Yakobson, M. Meyyappan, M. M. Rahman, P. M. Ajayan and V. Gadhamshetty, *ACS Nano*, 2020, **14**, 14809–14819.

27 Z. Li, S. Khuje, A. Chivate, Y. Huang, Y. Hu, L. An, Z. Shao, J. Wang, S. Chang and S. Ren, *ACS Appl. Electron. Mater.*, 2020, **2**, 1867–1873.
28 A. Sheng, S. Khuje, J. Yu, D. Petit, T. Parker, C.-G. Zhuang, L. Kester and S. Ren, *Nano Lett.*, 2021, **21**, 9279–9284.
29 B. K. Park, S. Jeong, D. Kim, J. Moon, S. Lim and J. S. Kim, *J. Colloid Interface Sci.*, 2007, **311**, 417–424.
30 J. Ramyadevi, K. Jeyasubramanian, A. Marikani, G. Rajakumar, A. A. Rahuman, T. Santhoshkumar, A. V. Kirthi, C. Jayaseelan and S. Marimuthu, *Parasitol. Res.*, 2011, **109**, 1403–1415.
31 J. Song, L. L. Wang, A. Zibart and C. Koch, *Metals*, 2012, **2**, 450–477.